

MAXIMAL DOMAIN INDEPENDENT REPRESENTATIONS IMPROVE TRANSFER LEARNING

Adrian Shuai Li
Purdue University
West Lafayette, IN
li3944@purdue.edu

Elisa Bertino
Purdue University
West Lafayette, IN
bertino@purdue.edu

Xuan-Hong Dang
IBM T.J. Watson Research Center
Yorktown Heights, NY
Xuan-Hong.Dang@ibm.com

Ankush Singla
Purdue University
West Lafayette, IN
asingla@purdue.edu

Yuhai Tu
IBM T.J. Watson Research Center
Yorktown Heights, NY
yuhai@us.ibm.com

Mark N Wegman
IBM T.J. Watson Research Center
Yorktown Heights, NY
wegman@us.ibm.com

ABSTRACT

State of the art domain adaptation involves the creation of (1) a domain independent representation (DIRep) trained so that from that representation it is not possible to determine whether the input is from the source domain or the target and (2) a domain dependent representation (DDRrep). The original input can then be reconstructed from those two representations. The classifier is trained only on source images using the DIRep. We show that information useful only in the source can be present in the DIRep, weakening the quality of the domain adaptation. To address this shortcoming, we ensure that DDRrep is small and thus almost all information is available in the DIRep. We use synthetic data sets to illustrate a specific weakness, which we call the hidden data effect, and show in a simple context how our approach addresses it. We further showcase the performance of our approach against state-of-the-art algorithms using common image datasets. We also highlight the compatibility of our model with pretrained models, extending its applicability and versatility in real-world scenarios.

1 INTRODUCTION

Labeling data for machine learning (ML) is a difficult and time-consuming process. In many instances, however, we may have labeled data similar to the data we are trying to label. It may be easier to label data in a related domain, which is more familiar to the labeler. We want to show how to leverage labeled data in a related domain.

In this paper, we propose an approach to address such question based on transferring knowledge between related domains, referred to as domain adaptation (DA) (Zhang & Gao, 2022; Zhang, 2021). In our setting, we have sufficient labeled data from a *source domain*. We are interested in assigning labels (from the set of labels in the source domain dataset) to data from a similar *target domain* with few or no labels. Examples of related domains are indoor vs outdoor pictures, summer vs winter pictures, or pictures with different resolutions. The source domain will generally have some information that is useful for labeling which is not available in the other domain. For instance, it is easier to identify ripe fruit in a color picture by using the color information than it might be in a target domain of grayscale pictures. Another general problem is that the characteristics of a domain may change over time. With older training samples, the test accuracy may deteriorate as the content of the domain evolves. DA uses information common to the different domains, hence it can be used for domains whose distribution changes over time.

One approach to achieve an effective DA is to generate a *domain-independent representation* (DIRep) of the data from different domains. A representation is domain-independent if one cannot determine from the representation which domain the information came from. If we can classify the objects from the source domain using only the DIRep, then there is a chance that we can classify objects in the target domain as well. To generate a DIRep, one method is to adversarially train two neural networks. The *generator* creates the DIRep, and the *discriminator* tries to identify whether the DIRep originally came from the source or target domains.

We can categorize the information passed from the generator to the classifier via the DIRep as deriving from the type of information commonly available in both domains as (CI), the type of information available typically only in the source as (SI), and information typically available only in the target as (TI). The *hidden data effect* occurs when the classifier

can utilize SI information despite the presence of the discriminator. Since the generator’s training is designed to aid the classifier’s performance solely in the source domain, it will try to “sneak” useful information past the discriminator. One way to evade the discriminator is for the generator, when observing data from the target, to synthesize random information that has similar statistics as those from the SI, and use it to masquerade as information that might have been from the source. Having target classifications rely on random information makes that classification less accurate, but the classification loss for the source, which is what the training is based on, improves.

To illustrate this, consider a scenario where we aim to classify images of dogs or wolves on the internet. Most pictures of wolves feature a snowy background, while a majority of dog pictures have a grassy background. Assume that is our source domain. If our target domain were images of canines at veterinary clinics, this spurious correlation between labels and background no longer holds. In this case, the generator can take advantage of the snowy background and places into the DIRep something that signifies “wolf”. If it sees a veterinarian’s background it randomly puts into the DIRep “wolf” or “dog”. This leaves the discriminator unable to distinguish the domain of the image. As a result, the random information introduced by the generator for the target domain data will reduce their classification accuracy.

To address the hidden data effect, VAEGAN uses a new model that combines a variational autoencoder (VAE) with the GAN-based adversarial learning approach. Classification is only based on the DIRep. In order to achieve more accurate DA, the DIRep should contain as much information as possible. This is achieved by introducing a minimal Domain-Dependent Representation (DDRep) to absorb all domain-specific information with the property that the concatenation of DDRep and DIRep is sufficient for data reconstruction. By training to minimize the KL divergence of the DDRep we ensure that the information in the DIRep is maximized as the two together are sufficient to recreate the input.

In VAEGAN, the generator is trained by four loss functions. Besides the classification loss (for the source domain), and the discriminator loss, it is also trained to minimize the reconstruction loss for both the source and target domains and the KL-divergence of the DDRep. As a result, the generator can no longer insert random results relevant to the source classification into the DIRep, since doing so would hurt the reconstruction on the target. Instead, the generator focuses on including information needed for reconstructing the image, which would be useful for accurate classification. In this way, VAEGAN can counteract the hidden data effect.

We empirically test VAEGAN thoroughly and show that our model is both less vulnerable to the hidden data effect and outperforms other algorithms in unsupervised domain adaptation. VAEGAN works well when the weights of the generator are initialized to the value of some pre-trained model. In the experiments section we show that we can learn to classify even when the source domain has very little data, by initializing the generator with values that classify to categories that are not in the source or target domains.

2 RELATED WORK

Transfer learning is an active research area that has been covered by several survey papers (Liu et al., 2022; Zhang & Gao, 2022; Zhang, 2021; Zhuang et al., 2020; Liu et al., 2019; Wang & Deng, 2018). These surveys categorize solutions into those relying on: data distribution discrepancy, pseudo-labeling, adversarial learning, reconstruction loss, and representation learning. Our solution falls in the intersection of adversarial learning, reconstruction loss and representation learning. We discuss the most relevant approaches in Sections 2.1 and 2.2.

2.1 ADVERSARIAL LEARNING BASED APPROACHES

These approaches typically aim at learning what we described as a DIRep by employing two competing networks of feature extractor/generator and domain discriminator. The domain adversarial neural network (DANN) (Ganin et al., 2016), one of the first such approach, uses three network components, namely a feature extractor, a label predictor and a domain classifier. The generator is trained in an adversarial manner to maximize the loss of the domain classifier by reversing its gradients. The generator is trained at the same time as the label predictor to create a DIRep that contains domain-invariant features for classification. The adversarial discriminative domain adaptation (ADDA) (Tzeng et al., 2017) approach adopts similar network components, yet its learning process involves multiple stages in training the three components of the model. Recently, Chadha et al. Chadha & Andreopoulos (2019) improve ADDA by extending the discriminator output over the source classes, in order to model the joint distribution over domain and task. Singla et al. (2020) has proposed a hybrid version of the DANN and ADDA where the generator is trained with the standard GAN loss function (Goodfellow et al., 2020). We refer to this as the GAN-based method (Singla et al., 2020). DANN and ADDA have recently been used based on pre-trained ResNet-50 models (Chen et al., 2020).

All adversarial learning based methods (DANN, ADDA and GAN-based) aim at learning a common representation feature space between the source and target domains. While they all achieved similar results in classification in the target domain, depending on details of the data and the networks, the DIRep may suffer from the aforementioned hidden data effect. Specifically, all these methods attempt to learn features that both fool the discriminator and lead an accurate classification for the source domain. Learning such features based purely on adversarial and supervised learning is challenging, since the features that can fool the discriminator may not lead to good classification, and vice versa. As we show in our experiments, such hidden data effect can degrade the classification performance in the target domain.

2.2 REPRESENTATION AND RECONSTRUCTION BASED APPROACHES

A leading approach in this category is the Domain Separation Networks (DSN) (Bousmalis et al., 2016). There are two extractors (generators) for each domain in DSN, one private and one shared, which create a private and a shared representation of the data corresponding to the DDRep and DIRep, respectively. The shared generator from the two domains is trained to produce a DIRep whose origins (source or target) cannot be determined. This shared generator hopefully captures the common features shared by the two domains. The shared and the private generators from each domain are trained to produce different results. Their DDRep and DIRep have the same shape, and they define a linear “soft subspace orthogonality constraint between the private and shared representation of each domain” to ensure that the DIRep and DDRep are as different as possible. The training of the shared generator in DSN is similar to the adversarial learning based approach. The new feature of DSN is the addition of a shared autoencoder that enforces the reconstruction of the data from the combined private and shared representations in each domain. At the same time, a classifier is trained from the shared representation (DIRep) of the source domain and the labels. Deep Reconstruction Classification Networks (DRCN) (Ghifary et al., 2016) is another approach that relies on reconstruction to learn a common encoding representation shared between the two data domains.

By including an autoencoder, approaches like DSN require that all information needed for reconstruction is in either the DDRep or DIRep. We do so as well. This aids classification. We will show that DSN outperforms adversarial learning based methods such as DANN and GAN-based algorithms (Singla et al., 2020).

While DSN uses loss functions to ensure the DIRep and DDRep are linearly different, we use either loss functions or explicit construction to ensure that the DDRep is small, and thus that the DIRep contains as much information as possible. In Section 3.2, we will describe why making sure that the DDRep is small is superior to ensuring that it is orthogonal and the same size as the DIRep.

3 THE VAEGAN FOR DOMAIN ADAPTATION

In this section we formulate our model that combines GAN-based DA with a variational autoencoder (VAE) to create a maximal DIRep for transfer learning. Fig. 1 shows the architecture of our model, referred to as VAEGAN.

(1) Networks. There are five neural networks (by neural network, we mean the network architecture and all its weights) in the algorithm: 1) G is the generator; 2) D is the discriminator; 3) C is the classifier; 4) E is the encoder; 5) F is the decoder.

(2) Inputs and outputs. The data is given by (x, l, d) where x is the input; we use the notation x^s and x^t to respectively represent the source and target data samples, when necessary to distinguish them. l is the label of sample x (if any), and d is the domain identity (e.g., can be as simple as one bit of 0 for the source domain and 1 for the target domain). In the zero-shot or few-shot domain adaptation settings, l is available for all source data samples, but none or only a few are known for the target samples. x is the input given to both encoder E and generator G . The DDRep and DIRep correspond to the intermediate outputs of E and G , respectively:

$$DDRep = E(x), \quad DIRep = G(x), \quad (1)$$

which then serve as the inputs for the downstream networks F , D , and C . In particular, DIRep serves as the input for D and C , and both DIRep and DDRep serve as the inputs for F . The outputs of these three downstream networks are \hat{x}

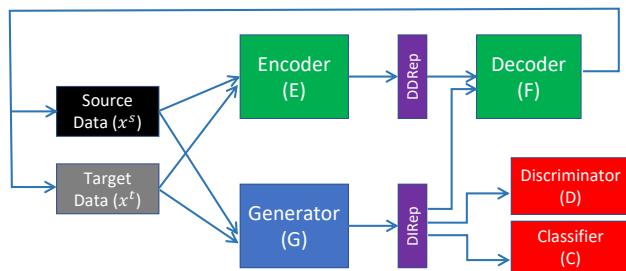


Figure 1: Architecture of VAEGAN.

from the decoder F ; \hat{d} from the discriminator D ; and \hat{l} from the classifier C . These outputs are:

$$\hat{x} = F(DDRep, DIRep) = F(G(x), E(x)), \hat{d} = D(DIRep) = D(G(x)), \hat{l} = C(DIRep) = C(G(x)), \quad (2)$$

where we list the dependence of the outputs on the corresponding networks explicitly.

(3) Loss functions. Some measures of the differences between the predictions from the networks, i.e., $(\hat{x}, \hat{d}, \hat{l})$ and their actual values (x, d, l) are used to construct the loss functions. Typically a loss function would take two arguments, a prediction and the actual label/value. We often use the name of the loss function without specifying the arguments, and do so for the discriminator, generator, classification and reconstruction losses. Like a variational autoencoder (VAE), we introduce an additional KL divergence loss function for E to create a minimal DDRep so we can force most of the input information into the DIRep. All the loss functions with their dependence on specific neural networks are given explicitly here: (1) Classification loss: $\mathcal{L}_c = \mathcal{L}_c(\hat{l}, l) = \mathcal{L}_c(C(G(x)), l)$. (2) Discriminator loss: $\mathcal{L}_d = \mathcal{L}_d(\hat{d}, d) = \mathcal{L}_d(D(G(x)), d)$. (3) For the generator loss, we want to train the generator to fool the discriminator. So, the generator has a smaller loss when the discriminator makes the wrong prediction: $\mathcal{L}_g = \mathcal{L}_g(\hat{d}, 1 - d) = \mathcal{L}_d(D(G(x)), 1 - d)$. (4) Reconstruction loss: $\mathcal{L}_r = \mathcal{L}_r(\hat{x}, x) = \mathcal{L}_r(F(G(x), E(x)), x)$. (5) KL loss for DDRep: $\mathcal{L}_{kl} = D_{KL}(Pr(E(x)) \parallel \mathcal{N}(0, I))$. For the reconstruction loss \mathcal{L}_r , we used the L_2 -norm. For $\mathcal{L}_d, \mathcal{L}_g, \mathcal{L}_c$, we used cross entropy. More details can be found in Appendix A.

(4) The back-prop based learning. The gradient-descent based learning dynamics for updating the five neural networks is described by the following equations:

$$\begin{aligned} \Delta G &= -\alpha_G \left(\lambda \frac{\partial \mathcal{L}_g}{\partial G} + \beta \frac{\partial \mathcal{L}_c}{\partial G} + \gamma \frac{\partial \mathcal{L}_r}{\partial G} \right), \quad \Delta C = -\alpha_C \frac{\partial \mathcal{L}_c}{\partial C}, \quad \Delta D = -\alpha_D \frac{\partial \mathcal{L}_d}{\partial D}, \\ \Delta E &= -\alpha_E \left(\frac{\partial \mathcal{L}_{kl}}{\partial E} + \mu \frac{\partial \mathcal{L}_r}{\partial E} \right), \quad \Delta F = -\alpha_F \frac{\partial \mathcal{L}_r}{\partial F}, \end{aligned}$$

where $\alpha_{C,D,E,F,G}$ are the learning rates for different neural networks. In our experiments, we often set them to the same value, but they can be different in principle. The other hyperparameters λ, β, γ , and μ are the relative weights of the loss functions. These hyperparameters are also useful to understand the different algorithms. In fact, $\gamma = 0$ corresponds to the GAN-based algorithm presented in Singla et al. (2020). As easily seen from the equations above, when $\gamma = 0$, the GAN-based algorithm decouples from the VAE based constraints.

3.1 THE EXPLICIT DDREP ALGORITHM

To make the DIRep contain as much information as possible, we introduce a simplified *explicit DDRep algorithm* without the encoder E and set the DDRep explicitly to be the domain label (bit) d , i.e., $DDRep = d$. A variant of this approach is to add d to the DDRep generated by the encoder. d is the simplest possible domain dependent information that could serve to filter out the domain dependent information from the DIRep.

We were surprised that in some cases the explicit DDRep performs as well as the VAEGAN. We think the VAEGAN is more general, which is why we focus on it. When doing experiments with the VAEGAN model we observed that the KL divergence of the DDRep corresponds to less than one bit measured as entropy. We believe that the DIRep ends up containing information to describe both the original data and some generated information describing an alternative as if it came from the other domain. Then the DDRep merely has enough information for the decoder to determine which information to use in reconstructing the original data.

One useful feature of this simplified algorithm is that it allows us to check the effect of the DDRep directly by flipping the domain bit ($d \rightarrow 1 - d$). We know the domain bit is effective in filtering out domain dependent information from the DIRep if the reconstructed image $\hat{x} = F(DIRep, 1 - d)$ resembles an image from the other domain as shown in Fig.2.

3.2 COMPARING VAEGAN TO DSN

Although DSN has an equivalent of DIRep and a DDRep, rather than forcing the DDRep to contain little information as in VAEGAN, it defines a linear orthogonality constraint between the private and shared representations of each domain. However, linear orthogonality in the high dimensional representation space is a weaker constraint as compared to that in VAEGAN that tries to minimize the DDRep to create the maximum DIRep. As a result, depending on the initiation, DSN may not lead to the maximum DIRep, which makes it more prone to the hidden data effect.

DSN and VAEGAN use different loss functions to determine what goes into the DDRep and DIRep: orthogonality in DSN; and minimization of the DDRep in VAEGAN. As we will show later in Section 4.3, the orthogonality loss function

used in DSN is less constraining on the optimal set of weights than the information minimization of VAEGAN. We will also show in that section that minimizing the DIRep instead of the DDRep as in VAEGAN, we can find solutions that are consistent with the orthogonality constraint of DSN but have poorer performance at domain adaptation. However, using the opposite of DSN’s orthogonality while consistent with VAEGAN’s minimization does not find bad solutions.

4 EXPERIMENTS

We now evaluate VAEGAN across different adaptation settings. We first demonstrate that in an artificial setting the hidden data effect takes place. Then we consider a more natural settings to show that we have a real advantage over a DANN like system and even a DSN like system. Since the generator and classifier topologies are the same in all of these systems, we need to show that the weights trained by VAEGAN are usually better. The other systems may occasionally have the same performance as VAEGAN. Thus we have used multiple runs and a z-score to assess whether one set of runs is statistically better than another.

Cheating is our technique for encouraging the hidden data effect. If you do a Google search for images of wolves, probably half of them are in snow. If you do a Google search for dogs, none of them are likely to be in snow. So if we want to classify dogs from wolves where the domain is images on the internet, snow is very helpful. But suppose you want to classify dogs from wolves in the results stemming from the query “animals in winter”. In that case, snow is useless. By adding information to enable a classifier of images to “cheat” by using useful information only available in one domain, we have found we encourage the hidden data effect. What we call cheating is a common problem that occurs in some natural DAs.

We construct several DA scenarios where some cheating clue exist in the source domain based on two widely used image datasets: (1) Fashion-MNIST¹, which consists of 60,000 grayscale images for training and 10,000 images for testing. Each image is represented as a 2-dimensional tensor of 28×28 and belongs to one of 10 classes; (2) CIFAR-10 dataset² which consists of 50,000 images for training and 10,000 images for testing from 10 classes. Each image is represented by a $32 \times 32 \times 3$ tensor (i.e., a color image with 3 channels of Red, Green and Blue).

We also validate our model on the standard benchmarks for unsupervised DA including MNIST (LeCun et al., 1998), MNIST-M (Ganin et al., 2016), Street View House Number (Netzer et al., 2011), synthetic digits (Ganin et al., 2016) and Office-31 (Saenko et al., 2010) for comparison against other state-of-the-art unsupervised DA approaches.

4.1 BENCHMARKS DEMONSTRATING HIDDEN DATA EFFECT

4.1.1 FASHION-MNIST CLASSIFICATION

Fashion-MNIST is a well known dataset, which we use as a source domain. We construct a target domain by flipping the images of 180° . To simulate shortcut information, we add to the source data set a one hot vector that contains the correct classification. We call that information cheating bits, because it is not available in the target domain. To the target dataset we also add some bits, but they either include information suggesting a random classification (random cheating), so the shortcut information is useless in the target domain or one that is shifted to the next label from the correct label (shift cheating), so it is always wrong, but perhaps in a predictable way. The one-hot bits have the same distribution in the source and target data sets, so if they are reflected in the DIRep the discriminator would not detect the difference between source and target. In this case, a classifier learned from this partial representation would perform poorly on the target data.

Benchmark algorithms We compare our method against the prevailing adversarial DA approaches in unsupervised setting: GAN-based approach (Singla et al., 2020), Domain-Adversarial Neural networks (DANN) (Ganin et al., 2016) and Domain Separation Networks (DSN) (Bousmalis et al., 2016). We implemented both VAEGAN and the explicit DDRep algorithm in the zero-shot setting. We only report the results about the explicit DDRep algorithm as it achieves almost identical performance on this task. We observe that the information content of the DDRep as determined by the KL divergence is usually less than 1 bit after training where DIRep retains the rest of the information. We also provide two baselines, a classifier trained on the source domain samples without DA (which gives us the lower bound on target classification accuracy) and a classifier trained on the target domain samples (which gives us the upper bound on target classification accuracy). We compare the mean accuracy of our approach and the benchmark unsupervised DA algorithms on the target test set in Table 1. The z-scores of comparing our method with other methods are shown

¹<https://github.com/zalandoresearch/fashion-mnist>

²<https://www.cs.toronto.edu/~kriz/cifar.html>

Table 1: Mean classification accuracy (%) of different adversarial learning based unsupervised DA approaches for the constructed Fashion-MNIST datasets.

Model	No cheating	Shift cheating	Random cheating
Source-only	20.0	11.7	13.8
GAN-based (Singla et al., 2020)	64.7	58.2	54.8
DANN (Ganin et al., 2016)	63.7	58.0	53.6
DSN (Bousmalis et al., 2016)	66.8	63.6	57.1
VAEGAN (explicit DDRRep)	66.9	66.8	61.6
Target-only	88.1	99.8	87.9

Table 2: Averaged classification accuracy (%) of different adversarial learning based unsupervised DA approaches for constructed CIFAR-10 dataset with a spectrum of bias.

Model	0% bias	20% bias	40% bias	60% bias	80% bias	90% bias	100% bias
Source-only	10.0	10.0	10.0	10.0	10.0	10.0	10.0
GAN-based (Singla et al., 2020)	63.0	62.5	61.4	56.9	53.2	44.5	30.1
DANN (Ganin et al., 2016)	62.7	62.0	61.0	56.5	52.2	42.9	29.1
DSN (Bousmalis et al., 2016)	68.7	67.9	67.3	67.5	64.5	61.7	32.2
VAEGAN	70.4	69.8	69.8	69.7	68.2	64.1	34.2
Target-only	78.9	78.9	78.9	78.9	78.9	78.9	78.9

in Figure 3. More details of the topology, learning rate, hyper-parameters setup and results analysis is provided in Appendix B.

The effect of single-bit DDRRep As we mentioned, the decoder learns to reconstruct the image by using DIRep and DDRep (domain bit) together. Figure 2 shows reconstructed images for the shift cheating scenario. The reconstructed images are a bit fuzzier and perhaps a bit more like generic images of elements in the same class. Some details seem to be getting lost despite the reconstruction. Nevertheless, the reconstructed images have rendered the domain bit effective in filtering out domain-dependent information, as the reconstructed images look like they are from the other domain when we flip the domain bit.

4.1.2 CIFAR-10 CLASSIFICATION

We are interested in more natural DA scenarios where the source and target images might be captured with different sensors and thus have different wavelengths and colors. To address this use case, we created our source and target datasets based on CIFAR-10 with different color planes. Furthermore, we introduced the cheating color plane where the choice of the color planes in the source data have some spurious correlation with the labels. We observe similar hidden data effect on the CIFAR-10 set with spurious correlation, suggesting that the optimization difficulties of previous methods and the results of our methods are not limited to a particular dataset.

The source set with cheating color planes is constructed as follows. First, we encode labels in CIFAR-10 with values between 0 and 9. Then for each CIFAR-10 image, if its label is odd, we keep only the B channel with prob p , and randomly keep the B or the R channel for the rest. Similarly, if the label is even, with prob p , the image has only the R channel, and either the R or B channel is kept for the rest. For example, when $p = 1$, all images with odd labels have only the B channel and all images with even labels have only the R channel. We call p the *bias* since it controls the strength of the spurious correlation between the color of the image and its label. In the target domain, for each CIFAR-10 image we keep only the G channel regardless of the label. We compare our approach and the others with p taking values from the set $\{0, 0.2, 0.4, 0.6, 0.8, 0.9, 1.0\}$. A larger value of p indicates a higher level of spurious correlation in the source data and thus a more challenging DA task.

In this “cheating-color-plane” setting, the GAN-like algorithms might cheat by leveraging the correlation between the presence or absence of the color planes and the label of the image to create an easier classification scheme for the labeled source data. Consequently, the DIRep would include false cheating clues which can degrade performance for the target data where the cheating clues lead to the wrong answer.

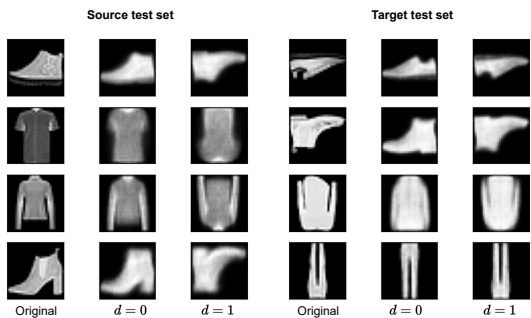


Figure 2: Columns 1 and 4, original images; 2 and 6, reconstructions of originals; 3 and 5, reconstructions with domain bit flipped.

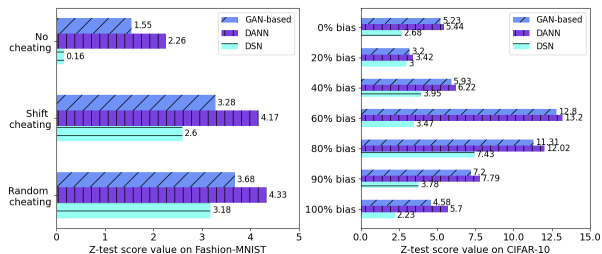


Figure 3: Z-test score value comparing VAEGAN to other models for constructed Fashion-MNIST (left) and CIFAR-10 (right). $Z > 2.3$ means the probability of VAEGAN being no better is ≤ 0.01 .

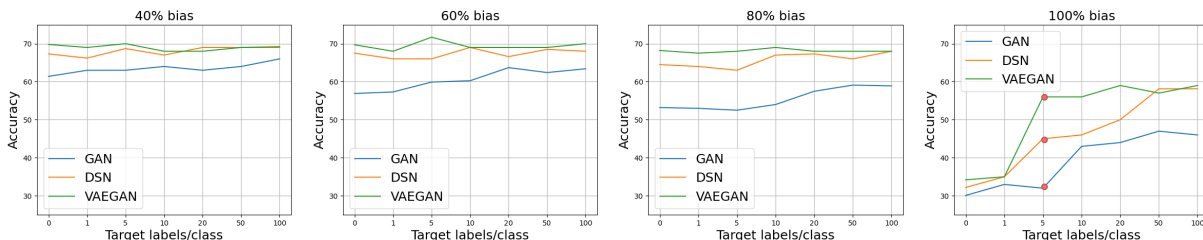


Figure 4: Mean classification accuracy on CIFAR-10 with semi-supervised setting for three different DA algorithms. Overall, a few target labels improve classification accuracy. The improvement is significant in 100% bias setting.

We report the mean accuracy of VAEGAN and the same benchmark algorithms on the target test set in Table 2. The z-scores of comparing our method with other methods are shown in Figure 3. The details of the experiment and analysis of the results are included in Appendix C.

4.1.3 SEMI-SUPERVISED DOMAIN ADAPTATION

As an additional experiment, we also evaluated the proposed algorithm for semi-supervised DA on the constructed CIFAR-10 datasets. The model is provided with a majority of unlabeled target data and a small amount of labeled target data. In our setting, we revealed 1, 5, 10, 20, 50 and 100 samples per class which we then used for contributing to the classification loss through the label prediction pipeline. We also provided the same number of labels for the GAN-based and DSN method. We skipped the DANN method since its performance is very similar to the GAN-based approach. More importantly, we ask the following question: *How much does each algorithm gain from a small labeled target training set for different biases?* The classification loss on the target ensures that the generator does not get away with learning a DRep that contains only the cheating clue, which could bias the model during training and cause a high classification loss.

We select four most representative biases and show the results in Figure 4. For 40%, 60% and 80% biases, the classification accuracy does improve, but not significantly as the number of target labels increases. The performance order of VAEGAN > DSN > GAN-based is preserved. When the bias is equal to 100%, the performance curves are quite different. All of them increase significantly with the number of target labels, while the order of performance is preserved. While all three algorithms benefit from a small number of target labeled samples, VAEGAN improves the most, surpassing DNS and GAN-based results by 12% and 25% respectively with only a total of 50 target labels (note that it corresponds to 5 labels/class in Figure 4).

4.2 STANDARD DA BENCHMARKS

There are two types of standard benchmark datasets: type-1 dataset presents the same information in a different form, perhaps changing color or line width; type-2 dataset contains additional information in one domain, like the presence of the background of the object, which is absent in the other. It is clear that type-2 dataset is prone to the hidden data effect while type-1 dataset is not. We applied VAEGAN in two representative benchmark datasets: the digits dataset and the

Table 3: Mean classification accuracy (%) of different adversarial learning based unsupervised DA approaches for the digits datasets. The results are cited from each study. * The results are replicated from DSN paper using the same regular MSE for reconstruction loss.

Model	MNIST to MNIST-M	Synth Digits to SVHN	SVHN to MNIST
Source-only	56.6	86.7	59.2
DANN (Ganin et al., 2016)	76.6	91.0	73.8
ADDA (Tzeng et al., 2017)	80.0	-	76.0
DSN* (Bousmalis et al., 2016)	80.4	89.0	79.5
VAEGAN	82.0	91.2	85.8
Target-only	98.7	92.4	99.5

Table 4: Mean classification accuracy (%) of different adversarial learning based unsupervised DA approaches for the office-31 dataset.

Model	$D \rightarrow A$	$W \rightarrow A$	$W \rightarrow D$	$A \rightarrow D$
Source-only	62.5	60.7	98.6	68.9
DANN (Ganin et al., 2016)	68.2	67.4	99.2	79.7
ADDA (Tzeng et al., 2017)	69.5	68.9	99.6	77.8
CDAN (Long et al., 2018)	70.1	68.0	100.0	89.8
GTA (Sankaranarayanan et al., 2018)	72.8	71.4	99.9	87.7
SimNet (Pineiro, 2018)	73.4	71.8	99.7	85.3
AFN (Xu et al., 2019)	69.8	69.7	99.8	87.7
Chadha et al. (Chadha & Andreopoulos, 2019)	62.2	-	-	80.9
IFDAN-1 (Deng et al., 2021)	69.2	69.4	99.8	80.1
VAEGAN	73.8	72.5	100.0	89.0

Office-31 dataset. We found that VAEGAN has a good performance comparable with other DA algorithms for the type-1 dataset while it outperforms other methods for the type-2 dataset as it eliminates the hidden data effect. We believe that outside of the setting of benchmarks there are many more type-2 datasets where VAEGAN has a clear advantage.

4.2.1 DIGITS DATASETS

In this experiment, we use three unsupervised domain adaptation pairs: 1) MNIST \rightarrow MNIST-M, 2) Synth Digits \rightarrow SVHN, and 3) SVHN \rightarrow MNIST. Example images from all four datasets are provided in Appendix D. The architecture and hyper-parameter settings are also provided in Appendix D due to a limit of space. Table 3 shows the results on the digits datasets. We cited the results from each study to make a fair comparison. In summary, VAEGAN outperforms all the other approaches we compared with for all three unsupervised DA scenarios.

4.2.2 OFFICE-31 DATASETS

The Office-31 dataset has 4110 images from 31 classes in three domains: amazon (2817 images), webcam (795 images) and dslr (498 images). The three most challenging domain shifts reported in previous works are dslr to amazon ($D \rightarrow A$), webcam to amazon ($W \rightarrow A$) and amazon to dslr ($A \rightarrow D$). In $D \rightarrow A$ and $W \rightarrow A$ are the cases with the least labelled information.

We follow the the previous work in Tzeng et al. (2017); Chen et al. (2020) which use a pretrained ResNet-50 on ImageNet (Deng et al., 2009) as a base. We present the results in Table 4. VAEGAN is competitive on this adaptation task, matching the performance of Long et al. (2018) in $A \rightarrow D$ and $W \rightarrow D$, and outperforming all the approaches in all other tasks. However, it’s worth noting that Long et al. (2018) utilizes a conditional discriminator conditioned on the cross covariance of domain-specific feature representations and classifier predictions, which has the potential to further enhance our results. We will leave exploring this possibility for future work. Our approach shows the most significant performance improvements in scenarios such as $D \rightarrow A$ and $W \rightarrow A$, in which background information is present within the D and W domains, while being absent in the A domain.

4.3 THE MUTUAL ABLATION EXPERIMENT BETWEEN DSN AND VAEGAN

To gain intuition for the difference between DSN and VAEGAN, we looked at a 3-D geometrical analogy of a representation decomposition as shown in Fig. 5 where source (S) and target (T) data represented in this analogy by vectors in 3D space are decomposed into the sum of DIRep (DI) and DDRep (DD): $S = DI_x + DD_x^S$, $T = DI_x + DD_x^T$ where the subscript x represents the DSN (D) and VAEGAN (V) algorithms, respectively. In DSN, the orthogonality constraint enforces $DI_D \perp DD_D^{S,T}$, which can be satisfied by any points on the blue circle in Fig. 5. In VAEGAN, however, the size of DDRep’s, i.e., $\|S - DI\| + \|T - DI\|$ is minimized leading to a unique solution DI_V (red dot in Fig. 5), which not only satisfies the orthogonality constraint ($DI_V \perp DD_V^{S,T}$) but also maximizes the DIRep ($\|DI_V\| \geq \|DI_D\|$) (see Appendix F for proof details).

To demonstrate the difference between DSN and VAEGAN, we designed a mutual ablation experiment. In DSN, the orthogonality constraint is enforced by a difference loss ($\mathcal{L}_{difference}$), while minimization of DDRep in VAEGAN is enforced by a KL loss (\mathcal{L}_{kl}).

We ask if we negate the $\mathcal{L}_{difference}$, does VAEGAN suffer? We also ask if we make the DIRep smaller rather than, as in VAEGAN, making the DDRep small, does DSN suffer? We refer to minimizing the information content of the DIRep as reverse \mathcal{L}_{kl} . The results are presented in the Table 5. These results show that by introducing an additional loss term in the DSN that gently pressures the system to minimize the information in the DIRep, the so called “DSN + reverse \mathcal{L}_{kl} ” method achieves sub-optimal domain adaptation than the original DSN. It also shows that even after this gentle pressure (perturbation) is removed (the “DSN*” method), optimal domain adaptation is not regained. Given that there can be many sub-optimal solutions due to the weak orthogonality constraint in DSN as illustrated in Fig. 5, this phenomenon probably happens because DSN found another sub-optimal solution from the initiation of weights reached by the gentle perturbation. On the contrary, the performance of VAEGAN is not affected by adding the reverse of $\mathcal{L}_{difference}$ in the “VAEGAN + reverse $\mathcal{L}_{difference}$ ” method. This is probably due to the fact that the DDRep-minimization in VAEGAN represents a much stronger constraint, which is not affected by the weaker reverse $\mathcal{L}_{difference}$.

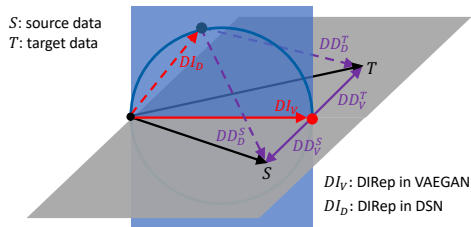


Figure 5: Schematic comparison between DSN and VAEGAN. See text and Appendix F for explanation.

Table 5: Effect of the reverse of \mathcal{L}_{kl} (VAEGAN) and the reverse of $\mathcal{L}_{difference}$ (DSN) to the other model. The first row is the DSN with the reverse \mathcal{L}_{kl} . In the second row, we remove the \mathcal{L}_{kl} after 10000 steps and resume the DSN training for another 10000 steps. The third row is replicated from Table 1. The values of other loss functions in DSN + reverse \mathcal{L}_{kl} and DSN* are similar to the ones in DSN. The fourth row is the VAEGAN with the reverse of $\mathcal{L}_{difference}$. The last row is the VAEGAN.

Methods	No cheating	Shift cheating	Random cheating
DSN + reverse \mathcal{L}_{kl}	61.2	59.5	53.8
DSN*	62.7	60.3	55.9
DSN	66.8	63.6	57.1
VAEGAN + reverse $\mathcal{L}_{difference}$	66.8	66.8	60.1
VAEGAN	66.9	66.8	61.6

5 CONCLUSION AND FUTURE WORK

In this paper, we described the challenges in DA caused by the hidden data effect and presented a better solution than previous methods for a number of common image datasets. The hidden data effect is more likely to appear in complex data problems, e.g., we see more of its impact in CIFAR than in Fashion-MNIST. The hidden data effect is also likely to appear when there is a drift in data, making classification more difficult. We showed that using a DIRep and DDRep trained with both a variational autoencoder and a discriminator makes a good base (DIRep) for a classifier, when we add pressure for the DDRep to be small. It would be interesting to test our method in these more complex problems.

In the case where there is a limited number of labeled samples, pseudo labelling is a very powerful technique that progressively adds more statistically likely labels (pseudo-labels) to the data (Chen et al., 2020; Zou et al., 2018). However, it depends on the accuracy of the initial estimate. If our initial estimate of the target label based on VAEGAN is

better than other algorithms then it is reasonable to expect that VAE_{GAN} could benefit from pseudo-labeling techniques. Indeed, combining pseudo-labeling techniques and VAE_{GAN} provides a promising direction for future work.

There is some exciting work on disentangled representations. The Interaction Information Auto-Encoder (IIAE) (Hwang et al., 2020) may have techniques for distinguishing the CI, TI and SI parts of the DIRep and perhaps making the CI bigger. But they do not do classification with domain adaptation. The Variational Disentanglement Network (VDN) (Hwang et al., 2020) attempts to generalize from a source domain without access to a target, and the Deep Adversarial Disentangled Autoencoder (DADA) (Peng et al., 2019) explores disentangled representations in the context of multiple different target domains.

Acknowledgments. This research has been funded by NSF under grants 2134667 “Privacy-Preserving Tiny Machine Learning Edge Analytics to Enable AI-Commons for Secure Manufacturing” and 2112471 “AI Institute for Future Edge Networks and Distributed Intelligence (AI-EDGE).” This research has also been partially sponsored by the U.S. Army Research Laboratory and the U.K. Ministry of Defence under Agreement Number W911NF-16-3-0001. The views and conclusions contained in this document are those of the authors and should not be interpreted as representing the official policies, either expressed or implied, of the U.S. Army Research Laboratory, the U.S. Government, the U.K. Ministry of Defence or the U.K. Government. The U.S. and U.K. Governments are authorized to reproduce and distribute reprints for Government purposes notwithstanding any copyright notation hereon.

REFERENCES

- Pablo Arbelaez, Michael Maire, Charless Fowlkes, and Jitendra Malik. Contour detection and hierarchical image segmentation. *IEEE transactions on pattern analysis and machine intelligence*, 33(5):898–916, 2010.
- Konstantinos Bousmalis, George Trigeorgis, Nathan Silberman, Dilip Krishnan, and Dumitru Erhan. Domain separation networks. *Advances in neural information processing systems*, 29, 2016.
- Aaron Chadha and Yiannis Andreopoulos. Improved techniques for adversarial discriminative domain adaptation. *IEEE Transactions on Image Processing*, 29:2622–2637, 2019.
- Minghao Chen, Shuai Zhao, Haifeng Liu, and Deng Cai. Adversarial-learned loss for domain adaptation. In *Proceedings of the AAAI conference on artificial intelligence*, volume 34, pp. 3521–3528, 2020.
- Jia Deng, Wei Dong, Richard Socher, Li-Jia Li, Kai Li, and Li Fei-Fei. Imagenet: A large-scale hierarchical image database. In *2009 IEEE conference on computer vision and pattern recognition*, pp. 248–255. Ieee, 2009.
- Wanxia Deng, Lingjun Zhao, Qing Liao, Deke Guo, Gangyao Kuang, Dewen Hu, Matti Pietikäinen, and Li Liu. Informative feature disentanglement for unsupervised domain adaptation. *IEEE Transactions on Multimedia*, 24: 2407–2421, 2021.
- Yaroslav Ganin, Evgeniya Ustinova, Hana Ajakan, Pascal Germain, Hugo Larochelle, François Laviolette, Mario Marchand, and Victor Lempitsky. Domain-adversarial training of neural networks. *The journal of machine learning research*, 17(1):2096–2030, 2016.
- Muhammad Ghifary, W Bastiaan Kleijn, Mengjie Zhang, David Balduzzi, and Wen Li. Deep reconstruction-classification networks for unsupervised domain adaptation. In *European conference on computer vision*, pp. 597–613. Springer, 2016.
- Ian Goodfellow, Jean Pouget-Abadie, Mehdi Mirza, Bing Xu, David Warde-Farley, Sherjil Ozair, Aaron Courville, and Yoshua Bengio. Generative adversarial networks. *Communications of the ACM*, 63(11):139–144, 2020.
- Kaiming He, Xiangyu Zhang, Shaoqing Ren, and Jian Sun. Deep residual learning for image recognition. In *Proceedings of the IEEE conference on computer vision and pattern recognition*, pp. 770–778, 2016.
- HyeongJoo Hwang, Geon-Hyeong Kim, Seunghoon Hong, and Kee-Eung Kim. Variational interaction information maximization for cross-domain disentanglement. *Advances in Neural Information Processing Systems*, 33:22479–22491, 2020.
- Sergey Ioffe and Christian Szegedy. Batch normalization: Accelerating deep network training by reducing internal covariate shift. In *International conference on machine learning*, pp. 448–456. PMLR, 2015.
- Yann LeCun, Léon Bottou, Yoshua Bengio, and Patrick Haffner. Gradient-based learning applied to document recognition. *Proceedings of the IEEE*, 86(11):2278–2324, 1998.

- Hong Liu, Mingsheng Long, Jianmin Wang, and Michael Jordan. Transferable adversarial training: A general approach to adapting deep classifiers. In *International Conference on Machine Learning*, pp. 4013–4022. PMLR, 2019.
- Xiaofeng Liu, Chaehwa Yoo, Fangxu Xing, Hyejin Oh, Georges El Fakhri, Je-Won Kang, Jonghye Woo, et al. Deep unsupervised domain adaptation: a review of recent advances and perspectives. *APSIPA Transactions on Signal and Information Processing*, 11(1), 2022.
- Mingsheng Long, Zhangjie Cao, Jianmin Wang, and Michael I Jordan. Conditional adversarial domain adaptation. *Advances in neural information processing systems*, 31, 2018.
- Yuval Netzer, Tao Wang, Adam Coates, Alessandro Bissacco, Bo Wu, and Andrew Y Ng. Reading digits in natural images with unsupervised feature learning. 2011.
- Xingchao Peng, Zijun Huang, Ximeng Sun, and Kate Saenko. Domain agnostic learning with disentangled representations. In *International Conference on Machine Learning*, pp. 5102–5112. PMLR, 2019.
- Pedro O Pinheiro. Unsupervised domain adaptation with similarity learning. In *Proceedings of the IEEE conference on computer vision and pattern recognition*, pp. 8004–8013, 2018.
- Kate Saenko, Brian Kulis, Mario Fritz, and Trevor Darrell. Adapting visual category models to new domains. In *Computer Vision—ECCV 2010: 11th European Conference on Computer Vision, Heraklion, Crete, Greece, September 5–11, 2010, Proceedings, Part IV 11*, pp. 213–226. Springer, 2010.
- Swami Sankaranarayanan, Yogesh Balaji, Carlos D Castillo, and Rama Chellappa. Generate to adapt: Aligning domains using generative adversarial networks. In *Proceedings of the IEEE conference on computer vision and pattern recognition*, pp. 8503–8512, 2018.
- Ankush Singla, Elisa Bertino, and Dinesh Verma. Preparing network intrusion detection deep learning models with minimal data using adversarial domain adaptation. In *Proceedings of the 15th ACM Asia Conference on Computer and Communications Security*, pp. 127–140, 2020.
- Eric Tzeng, Judy Hoffman, Kate Saenko, and Trevor Darrell. Adversarial discriminative domain adaptation. In *Proceedings of the IEEE conference on computer vision and pattern recognition*, pp. 7167–7176, 2017.
- Mei Wang and Weihong Deng. Deep visual domain adaptation: A survey. *Neurocomputing*, 312:135–153, 2018.
- Ruijia Xu, Guanbin Li, Jihan Yang, and Liang Lin. Larger norm more transferable: An adaptive feature norm approach for unsupervised domain adaptation. In *Proceedings of the IEEE/CVF international conference on computer vision*, pp. 1426–1435, 2019.
- Lei Zhang and Xinbo Gao. Transfer adaptation learning: A decade survey. *IEEE Transactions on Neural Networks and Learning Systems*, 2022.
- Youshan Zhang. A survey of unsupervised domain adaptation for visual recognition. *arXiv preprint arXiv:2112.06745*, 2021.
- Fuzhen Zhuang, Zhiyuan Qi, Keyu Duan, Dongbo Xi, Yongchun Zhu, Hengshu Zhu, Hui Xiong, and Qing He. A comprehensive survey on transfer learning. *Proceedings of the IEEE*, 109(1), 2020.
- Yang Zou, Zhiding Yu, BVK Kumar, and Jinsong Wang. Unsupervised domain adaptation for semantic segmentation via class-balanced self-training. In *Proceedings of the European conference on computer vision (ECCV)*, pp. 289–305, 2018.

A MORE DETAILS ON LOSS FUNCTIONS

Our code is available at (<https://anonymous.4open.science/r/Maximal-Domain-Independent-Representations-Improve-Transfer-Learning-A422/README.md>).

We provide the details of all the loss functions mentioned in Section 3 of the main paper. Recall that the data is given by (x, l, d) where x is the input with x^s and x^t representing the source and target data, respectively. l is the label of the sample, and d is the domain identity.

In unsupervised domain adaptation, the classification loss applies only to the source domain and it is defined as follows:

$$\mathcal{L}_c = - \sum_{i=1}^{N_s} l_i^s \cdot \log \hat{l}_i^s \quad (3)$$

where N_s represents the number of samples from the source domain, l_i^s is the one-hot encoding of the label for the source input x_i^s and \hat{l}_i^s is the softmax output of $C(G(x_i^s))$.

The discriminator loss trains the discriminator to predict whether the D_IRep is generated from the source or the target domain. N_t represents the number of samples from target domain and \hat{d}_i is the output of $D(G(x_i))$.

$$\mathcal{L}_d = - \sum_{i=1}^{N_s+N_t} \left\{ d_i \log \hat{d}_i + (1 - d_i) \log(1 - \hat{d}_i) \right\} \quad (4)$$

The generator loss is the GAN loss with inverted domain truth labels:

$$\mathcal{L}_g = - \sum_{i=1}^{N_s+N_t} \left\{ (1 - d_i) \log \hat{d}_i + d_i \log(1 - \hat{d}_i) \right\} \quad (5)$$

For the reconstruction loss, we use the standard mean squared error loss calculated from both domains:

$$\mathcal{L}_r = \sum_i^{N_s} \|x_i^s - \hat{x}_i^s\|_2^2 + \sum_i^{N_t} \|x_i^t - \hat{x}_i^t\|_2^2 \quad (6)$$

where $\hat{x}_i^s = F(G(x_i^s), E(x_i^s))$ and $\hat{x}_i^t = F(G(x_i^t), E(x_i^t))$

Finally, the KL-divergence loss measures the distance between the distribution of DDRep which comes from a Gaussian with mean $\mathbb{E}(DDRep)$ and variance $\mathbb{V}(DDRep)$ and the standard normal distribution.

$$\mathcal{L}_{kl} = D_{KL}(Pr(DDRep) \parallel \mathcal{N}(0, I)) = -\frac{1}{2}(1 + \log[\mathbb{V}(DDRep)] - \mathbb{V}(DDRep) - \mathbb{E}(DDRep)^2)$$

B EXPERIMENT DETAILS FOR FASHION-MNIST

B.1 NETWORK ARCHITECTURE

All the methods are trained using the Adam optimizer with the learning rate of $2e - 4$ for 10,000 iterations. We use batches of 128 samples from each domain for a total of 256 samples. When training with our model (VAEGAN), the label prediction pipeline (generator and classifier) has eight fully connected layers (FC1, ..., FC7, FC_OUT). The number of neurons in FC1-4 is 100 for each layer. FC5 is a 100-unit layer that generates D_IRep, followed by two 400-unit layers (FC6-7). FC_OUT is the output layer for label prediction. The discriminator and decoder each have four layers with 400 hidden units and followed by the domain prediction layer and reconstruction layer, respectively. The encoder has two layers with 400 units, followed by 1-unit z_mean , 1-unit $z_variance$, and 1-unit sampling layer. Each of the 400-unit layers uses a ReLU activation function.

All the other models have the same architecture as VAEGAN when applicable. For the GAN-based approach and DANN, we turn off the decoder and corresponding losses. For the DSN, we keep the same network architecture for common networks and use \mathcal{L}_g for the similarity loss. Furthermore, we implement the shared and private encoders with same shape output vectors (Bousmalis et al., 2016).

B.2 HYPERPARAMETERS

As suggested in previous work (Ganin et al., 2016), the coefficient of the loss, which encourages domain invariant representation, should be initialized as 0 and changed to 1. We use the following schedule for the coefficient of \mathcal{L}_g in all the experiments where t is the training iteration:

$$\lambda = \frac{2}{1 + \exp(-t)} - 1 \quad (7)$$

Table 6: Mean classification accuracy (%) of different adversarial learning based unsupervised DA approaches for the constructed Fashion-MNIST datasets.

Model	No cheating	Shift cheating	Random cheating
Source-only	20.0	11.7	13.8
GAN-based (Singla et al., 2020)	64.7	58.2	54.8
DANN (Ganin et al., 2016)	63.7	58.0	53.6
DSN (Bousmalis et al., 2016)	66.8	63.6	57.1
VAEGAN	66.9	66.8	61.6
Target-only	88.1	99.8	87.9

Table 7: Z-test score value comparing VAEGAN to other models for constructed Fashion-MNIST. $z > 2.3$ means the probability of VAEGAN being no better is ≤ 0.01 .

Model	No cheating	Shift cheating	Random cheating
GAN-based (Singla et al., 2020)	1.55	3.28	3.68
DANN (Ganin et al., 2016)	2.26	4.17	4.33
DSN (Bousmalis et al., 2016)	0.16	2.60	3.18

The increasing coefficient allows the discriminator to be less sensitive to noisy signals at the early stages of the training procedure. For other hyperparameters, we used $\beta = 1, \gamma = \mu = 1$ (the hyperparameters were not tuned using validation samples).

We closely follow the setup of weights of the loss functions used in the DSN paper (Bousmalis et al., 2016) and DANN paper (Ganin et al., 2016). To boost the performance of DSN, we set the coefficient of \mathcal{L}_{recon} to 0.15 and the coefficient of \mathcal{L}_{diff} to 0.05, tuned parameter values determined by Bousmalis et al. (2016) using a validation set of target labels.

B.3 RESULTS AND ANALYSIS.

Table 6 summarizes the mean classification accuracy of different approaches for three cheating scenarios. In the no cheating scenario, we use the original Fashion-MNIST as source and flip the Fashion-MNIST for the target. We report the z-score of the comparison of the mean classification accuracy of our method with the mean classification accuracy of other methods over five independent runs (see Table 7). The higher the z-score, the more statistical confidence we should have that our method outperforms the other methods. A z-score of 2.33 corresponds to 99% confidence that our method is superior, assuming that the accuracy over different runs will follow a Gaussian distribution.

In the no cheating scenario, VAEGAN outperforms GAN-based and DANN and matches the result of DSN. The performance of GAN-based and DANN results in a 5% accuracy drop for the shift cheating and 10% drop for the random cheating. This validates our concern with the hidden data effect. The source cheating bits can be picked up in the DIRep as they represent an easy solution for the classifier that is trained only with source samples. If that is the case, then the cheating generator would perform poorly for the target domain, which has different cheating bits. Our method has only 0.1% and 5% accuracy drop respectively and is less vulnerable to the hidden data effect. As a reconstruction-based method, DSN performs better in the presence of cheating bits. In the shift and random cheating, our approach significantly outperforms DSN with a z-score of 2.60 and 3.18 respectively, which shows the correctness of our intuition that penalizing the size of DDRep can result in transferring as much information as possible to the DIRep. In the explicit DDRep algorithm, the DDRep is minimal as it only contains the domain label. Given a richer DIRep, our method leads to a classifier based on the invariant features of the images, which improves its performance on the target data.

C EXPERIMENT DETAILS FOR CIFAR-10

C.1 NETWORK ARCHITECTURE AND TRAINING PROCEDURE

When training with our approach, we implement the network components as deep residual neural networks (ResNets) with short-cut connections (He et al., 2016). ResNets are easier to optimize, and sometimes gain accuracy from increased depth. For our approach, we implemented the full-fledged VAEGAN and we added the domain label to the

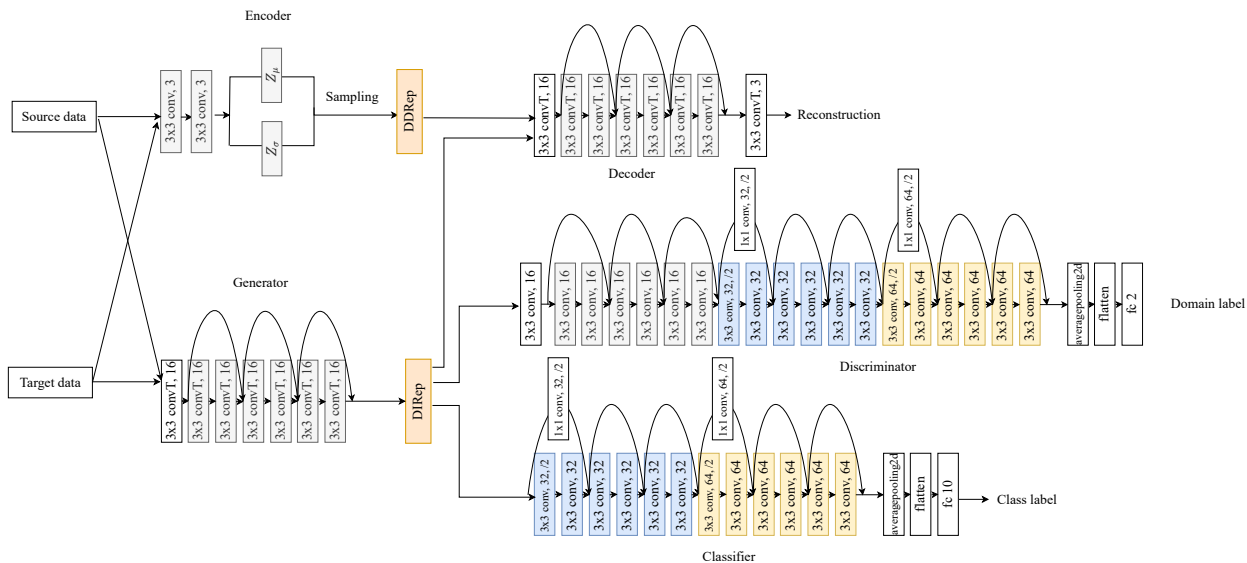


Figure 6: CIFAR10 architecture; inspired by the classical ResNet-20 (He et al., 2016)

DDRep generated by the encoder. The architecture is shown in Figure 6. The label prediction pipeline is adopted from the ResNet 20 for CIFAR-10 in He et al. (2016). For the generator, the first layer is 3×3 convolutions. Then we use a stack of 6 layers with 3×3 convolutions on the feature maps of size 32. The numbers of filters are 16. The architecture of the classifier consists of a stack of 6×2 layers with 3×3 convolutions on the feature maps of sizes $\{16, 8\}$ respectively. To maintain the network complexity, the number of filters are $\{32, 64\}$. The classifier ends with a global average pooling, and a fully-connected layer with softmax.

For the discriminator, the network inputs are $32 \times 32 \times 16$ domain invariant features. The first layer is 3×3 convolutions. Then we use a stack of 6×3 layers with 3×3 convolutions on the feature maps of sizes 32, 16, and 8 respectively, with 6 layers for each feature map size. The numbers of filters is $\{16, 32, 64\}$ respectively. The discriminator ends with a global average pooling, a 2-way fully-connected layer, and softmax.

The encoder has 4 convolutional layers: three 3×3 filters, two 3×3 filters (z mean) and two 3×3 filters (z variance) respectively. A sampling layer is also implemented which outputs the DDRep from the latent distribution z . The decoder learns to reconstruct an input image by using its DRep, DDRep and domain bit together. Hence, the inputs of the decoder are $32 \times 32 \times 19$ concatenated representations. The configuration of the decoder is the inverse of that of the generator.

We implemented the same ResNet-based architecture for all other approaches (when applicable). We use a weight decay of 0.0001 and adopt the BN (Ioffe & Szegedy, 2015) for all the experiments. The hyperparameters are the same as the ones in Section B.2.

C.2 RESULTS AND ANALYSIS

We report the mean accuracy of different unsupervised DA methods and our approach on the target test set in Table 8. The z-scores of comparing our method with other methods are shown in Table 9.

For all the DA tasks with varying biases, we observe that our approach outperforms the other approaches in terms of accuracy in the target set. This improvement is most pronounced when the source set has 60% and 80% bias levels, which means that over half of the source data has a spurious correlation between their color planes and labels. The poor performance of the GAN-based and DANN approaches is another example where the generator in these approaches learns a DRep that depends on the spurious correlation. This false representation leads to an issue similar to over-fitting where the model performs well on the source data, but does not generalize well on the target data in which the same correlation does not exist. In the DSN approach, the shared representation contains some domain-independent information other than the cheating clues which helps classification in the target domain.

Table 8: Averaged classification accuracy (%) of different adversarial learning based unsupervised DA approaches for constructed CIFAR-10 dataset with a spectrum of bias.

Model	0% bias	20% bias	40% bias	60% bias	80% bias	90% bias	100% bias
Source-only	10.0	10.0	10.0	10.0	10.0	10.0	10.0
GAN-based (Singla et al., 2020)	63.0	62.5	61.4	56.9	53.2	44.5	30.1
DANN (Ganin et al., 2016)	62.7	62.0	61.0	56.5	52.2	42.9	29.1
DSN (Bousmalis et al., 2016)	68.7	67.9	67.3	67.5	64.5	61.7	32.2
VAEGAN	70.4	69.8	69.8	69.7	68.2	64.1	34.2
Target-only	78.9	78.9	78.9	78.9	78.9	78.9	78.9

Table 9: z-test score value comparing VAEGAN to other models for constructed CIFAR-10. $z > 2.3$ means the probability of VAEGAN being no better than the other models is ≤ 0.01 .

Model	0% bias	20% bias	40% bias	60% bias	80% bias	90% bias	100% bias
GAN-based (Singla et al., 2020)	5.23	3.20	5.93	12.8	11.31	7.20	4.58
DANN (Ganin et al., 2016)	5.44	3.42	6.22	13.2	12.02	7.79	5.70
DSN (Bousmalis et al., 2016)	2.68	3.00	3.95	3.47	7.43	3.78	2.23

D SVHN, MNIST, MNIST-M AND SYNTH DIGITS

We evaluate the empirical performance of VAEGAN on four widely used domain adaptation benchmarks: MNIST (LeCun et al., 1998), MNIST-M (Ganin et al., 2016), Street View House Number (Netzer et al., 2011) and synthetic digits (Ganin et al., 2016). We use three unsupervised domain adaptation pairs: 1) MNIST \rightarrow MNIST-M, 2) Synth Digits \rightarrow SVHN, and 3) SVHN \rightarrow MNIST. Example images from all four datasets are provided in Figure 7. We implement our CNN topology based on the ones used in (Bousmalis et al., 2016) and (Ganin et al., 2016). We used Adam with the learning rate of 0.0002 for 25,000 iterations. The batch size is 128 for each domain. We did not use validation samples to tune hyperparameters. To make fair comparisons, we follow the instructions in (Bousmalis et al., 2016) and activate the \mathcal{L}_g after 20,000 steps of training. For other hyperparameters, we used $\beta = 1$, $\gamma = 1$, and $\mu = 1$.

MNIST to MNIST-M. We use the MNIST dataset as the source domain, and a variation of MNIST called MNIST-M as the target. MNIST-M was created by blending digits from the original MNIST set over patches randomly extracted from color photos from BSDS500 (Arbelaez et al., 2010).

Synthetic Digits to SVHN. This scenario is widely used to demonstrate the effectiveness of the algorithm when training on synthetic data and testing on real data. We use synthetic digits as the source and Street-View House Number data set SVHN as the target.

SVHN to MNIST. In this experiment, we further increase the gap between the two domains. The digit shapes in SVHN are quite distinct from those handwritten digits in MNIST. Furthermore, SVHN contains significant image noise, such as multiple digits in one image and blurry background.

E OFFICE DATASET

Our method was evaluated on the Office dataset, which comprises three distinct domains: Amazon, DSLR, and Webcam. Unlike larger datasets, the Office dataset is relatively small, containing only 2817 labeled images across 31 different categories in the largest domain. Due to the limited data availability, we opted to utilize the ResNet-50 architecture pretrained on the ImageNet dataset as the generator, following a common approach in recent domain adaptation studies (Tzeng et al., 2017; Chen et al., 2020). This choice allowed us to leverage the knowledge gained from ImageNet’s large-scale dataset and apply it to our specific domain adaptation task. We used Adam with the learning rate of 0.0002. The batch size is 16 for each domain. We did not use validation samples to tune hyperparameters. We used $\lambda = 0.1$, $\beta = 1$, $\gamma = 0.05$, and $\mu = 1$.

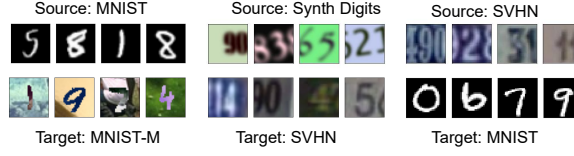


Figure 7: Example images from four domain adaptation benchmark datasets for three scenarios.

F THE GEOMETRICAL INTERPRETATION OF VAEGAN VERSUS DSN

To gain intuition for the difference between DSN and VAEGAN, we looked at a 3-D geometrical interpretation of representation decomposition as shown in Fig. 5 in the main text. Here, we show that all points on the blue circle satisfy the orthogonal condition, i.e., $DI_D \perp DD_D^{S,T}$.

The source and target data are represented by two vectors $S = \overrightarrow{OS}$, $T = \overrightarrow{OT}$ where O is the origin as shown in Fig. 8. We assume the source and target vectors have equal amplitude $|\overrightarrow{OS}| = |\overrightarrow{OT}|$. Let us define the plane that passes through the triangle $O - S - T$ as plane- \mathcal{A} (the gray plane in Fig. 8). The mid-point between S and T is denoted as V . Let us draw another plane (the blue plane- \mathcal{B}) that passes through the line OV and is perpendicular to the plane- \mathcal{A} . The blue circle is on the blue plane- \mathcal{B} with a diameter given by OV . Denote an arbitrary point on the blue circle as D with the angle $\angle DVO = \theta$. Let us define the plane that passes through the triangle $D - S - T$ as plane- \mathcal{C} (not shown in Fig. 8).

Since the blue plane- \mathcal{B} is the middle plane separating S and T , we have $ST \perp OV$ and $ST \perp DV$ (note that XY represents the line between the two points X and Y). Therefore, the line ST is perpendicular to the whole plane- \mathcal{B} : $ST \perp \mathcal{B}$, which means that ST is perpendicular to any line on plane- \mathcal{B} . Since the line DV is on the plane- \mathcal{B} , we have $OD \perp ST$. Since OV is a diameter of the blue circle, we have $OD \perp DV$. Since DV and ST span the plane- \mathcal{C} , we have OD is perpendicular to the whole plane- \mathcal{C} : $OD \perp \mathcal{C}$, which means that OD is perpendicular (orthogonal) to any line on plane- \mathcal{C} including DS and DT . Therefore, we have proved: $OD \perp DS$, $OD \perp DT$.

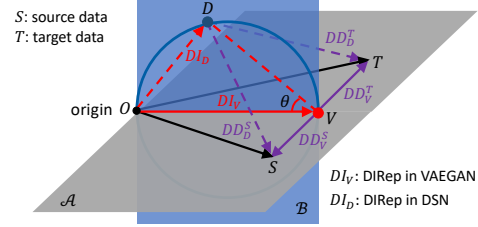


Figure 8: Schematic comparison between DSN and VAEGAN.

Note that with the notation given here we can express the DIRep and DDRep's for VAEGAN (V) and DSN (D) as:

$$\begin{aligned} DI_V &= \overrightarrow{OV}, \quad DD_V^S = \overrightarrow{VS}, \quad DD_V^T = \overrightarrow{VT}. \\ DI_D &= \overrightarrow{OD}, \quad DD_D^S = \overrightarrow{DS}, \quad DD_D^T = \overrightarrow{DT}. \end{aligned}$$

Since we have proved that $OD \perp DS$, $OD \perp DT$ for any point D on the blue circle, this means that any point on the blue circle satisfies the orthogonality constraint $DI_D \perp DD_D^{S,T}$.

In VAEGAN, the size of DDRep's, i.e., $\|S - DI\| + \|T - DI\| = (\|\overrightarrow{VS}\|^2 + \|\overrightarrow{DV}\|^2)^{1/2} + (\|\overrightarrow{VT}\|^2 + \|\overrightarrow{DV}\|^2)^{1/2}$ is minimized leading to a unique solution DI_V shown as the red dot (point V) in Fig. 8, which satisfies the orthogonality constraint ($DI_V \perp DD_V^{S,T}$) as it is on the blue circle. More importantly, the VAEGAN solution is unique as it maximizes the DIRep ($\|DI_V\| \geq \|DI_D\|$). This can be seen easily as follows. Given the angle $\angle DVO = \theta$, we have $\|DI_D\| = \|DI_V\| \sin \theta \leq \|DI_V\|$.